Hydroelastic response of wind-tracing floating offshore structures to irregular waves and wind

Lamei, Azin; Hayatdavoodi, Masoud; Riggs, H. Ronald

Publication date:
2022

Document Version
Peer reviewed version

9^{th} *International Conference on* HYDROELASTICITY IN MARINE TECHNOLOGY
Rome, Italy, July 10^{th}-13^{th} *2022*

Hydroelastic Response of Wind-tracing Floating Offshore Structures to Irregular Waves and Wind

Lamei, A.[1], Hayatdavoodi, M.[1,2*] and Riggs, H. R. [3]

[1] School of Science and Engineering, University of Dundee, Dundee DD1 4HN, UK
[2] College of Shipbuilding Engineering, Harbin Engineering University, Harbin 150001, China
[3] Civil and Environmental Engineering Department, University of Hawaii, Honolulu, Hawaii 96822, USA

Abstract. Motion and hydroelastic responses of floating offshore wind turbines (FOWT) to irregular waves and wind loads are studied by use of a numerical coupling approach in frequency domain. The hydrodynamic and aerodynamic loads on the structure are obtained by linear wave diffraction theory and the steady blade element momentum method, respectively, and the structural responses are computed by finite element method. Rigid body responses of a SPAR to combined irregular waves (JONSWAP spectrum) and steady wind are computed and compared with existing laboratory measurements. Good agreement between the computed responses of the structure and existing laboratory data is observed. Next, the rigid and hydroelastic responses of a new concept of FOWT, where multiple towers are placed on the floating platform, to irregular waves and wind are studied. The FOWT consists of an equilateral triangular platform that supports three 5 MW NREL wind turbines on its corners. The FOWT is attached to the seabed with turret-bearing system that allows for the rotation of the structure in response to environmental loads, hence wind-tracing FOWT. It is found that the hydroelastic motions of the wind-tracing FOWT results in significant changes on its heave and pitch responses compared with its rigid body motions.

Key words: *Offshore wind energy, Hydroelasticity, Aeroelasticity, Floating offshore wind turbines*

1. Introduction

Determining the complex dynamics of a FOWT due to the environmental loads, namely waves, current and wind loads is challenging. The aerodynamic loads on the rotor and the tower, the hydrodynamic loads of waves and current on the substructure and the mooring lines, and the restoration forces by the mooring lines on the structure results in coupled motions and deformations of a FOWT. For instance, the aerodynamic load on the rotor of a FOWT is influenced by the motion of its substructure, *i.e.* the motions of the platform impacts the direction of the incoming flow to the rotor, hence the power production and the efficiency of the wind turbine. Furthermore, elasticity of the blades, tower, and the substructure can significantly influence the responses of a FOWT to the environmental loads.

Several numerical coupling approaches have been developed to approximate the environmental loads and the motions of a FOWT. Commonly, the coupling numerical tools are limited to elasticity analysis of mainly the rotor and the tower, see [1] and [2] among others. However, possible resonant behaviour of the substructure might occur if the natural frequencies of the floating structure falls near or within the wave energy spectrum resulting in structural deformations. Therefore, the coupling between the elasticity of the entire structure and the environmental loads should be considered. Hydroelastic analysis is also required when we are interested in structural analysis (e.g. determining the stress and deformations). A multi-unit FOWT is an emerging concept in offshore wind energy, see for instance [3], [4] and [5]. The

*Correspondence to: mhayatdavoodi@dundee.ac.uk

multi-unit FOWTs consist of a large platform that supports several wind turbines on it. Due to the large size of the substructure, the elastic responses of the structure are particularly of significant importance and must be considered to obtain their motions to the environmental loads.

In a common approach for hydroelasticity analysis of FOWTs, the hydrodynamic loads on the structure are computed with linear potential flow theory and the mode-shapes of the structure are obtained with finite element method. The mode-shapes represent the flexibility of the FOWT and are added as generalized modes to the rigid body responses of the structure. The equation of motions of the FOWT are solved in time- or frequency domain for the rigid-body and generalized modes of the structure; see e.g. [6] and [4]. A recent review on motion and elasticity analysis of FOWTs is presented in [7] among others.

A fully coupled aero-hydro-elastic numerical tool is developed to obtain the elastic motions of a FOWT to the environmental loads. First, the theory and the numerical approach applied in this study are described. Next, as a benchmark study, the significant motions of a SPAR FOWT to irregular waves and combined irregular waves and wind are obtained and compared with available laboratory measurements and numerical solutions. Finally, the wind-tracing FOWT is described and its rigid- and flexible-body motions to waves and combined wave and wind loads are presented. The significant motions of the structure to irregular wave, and irregular waves and wind are presented for a range of incoming wave heading angles. Finally, discussion and concluding remarks regarding the presented analysis in this study are provided.

2. Theory $\&$ the numerical approach

The hydro- and aeroelasticity analysis of a FOWT to combined waves and wind loads are discussed thoroughly in [8]. In this section the theory and the formulations are briefly presented and the numerical solution is described.

An earth-fixed coordinate system is chosen with *x*- and *y*-axis on the still water level and *z*-axis pointing upwards. The motions in the *x*-, *y*- and *z*-directions are surge, sway and heave, respectively and the rotations about the *x*-, *y*- and *z*-axis are roll, pitch and yaw, respectively.

The wave-interaction with the substructure of a FOWT is studied by linear diffraction wave theory. In this approach, the total load on the substructure is the sum of the external hydrodynamic pressure force and the hydrostatic and mooring lines' restoration forces. The equation of motion of a floating structure in the absence of wind is,

$$\xi_j[-\omega^2(M_{ij}+a_{ij})+i\omega(\,b_{ij})+(\,c_{ij,moor}\,+\,c_{ij})]\;=\;AX_i,\quad i,j=1,2,\cdots 6, \tag{1}$$

where ω is the wave frequency and ξ_j is the complex body response phasor in mode j. M_{ij} is the modal structural mass matrix, and a_{ij}, b_{ij} and c_{ij} are the added mass, hydrodynamic damping and hydrostatic stiffness coefficient matrices, respectively. X_i is the amplitude of wave excitation force divided by the wave amplitude A and is presented in complex form. The mooring lines are modelled as springs with restoring coefficients of $c_{ij,moor}$.

The aerodynamic load on the rotor of a FOWT is computed by blade element momentum method (BEM). In this study, with a focus on quasi-steady aerodynamic loads on the rotor, the wind speed is constant and the incoming wind is in *x*-direction and axisymmetric with respect to the rotor. The thrust force on the rotor of a FOWT is a function of the incoming wind speed and the relative motion of the rotor along the direction of the incoming wind,

$$T(V_{rel})=\frac{1}{2}\rho A_r C_T(V_{\text{rel}}^2), \tag{2}$$

where ρ is the air density, A_r is the projected rotor area, and C_T is the thrust coefficient. Moreover, V_{rel} is the relative incoming wind speed to the rotor and is computed as $V_{\text{rel}}=V_0-V_h$ with V_0 and V_h are the incoming wind speed and the *x*-component of the structure velocity at the hub centre, respectively. In

frequency domain, assuming that the motion of the structure due to the incoming wind is restricted to the *xz*-plane, the *x*-component of the V_h is $i\omega(\xi_1+\xi_5(z_h-z_{cg}))$, where z_h and z_{cg} are the vertical coordinates at the hub and the centre of gravity, respectively. Equation (2) with small V_h can be approximated with Taylor series,

$$T(V_{rel}) = \frac{1}{2}\rho A_r C_T(V_0^2) - \rho A_r C_T(V_0\ i\omega(\xi_1 + \xi_5(z_h - z_{cg}))). \tag{3}$$

Equation (3) indicates that the total thrust force on a FOWT is the sum of excitation force by the incoming wind on a fixed rotor, the first term on the right-hand side and the harmonic force by the aerodynamic damping effect due to the relative motions of the structure along the direction of the incoming wind, the second term. The aerodynamic damping force can be rewritten as $i\omega(\xi_1 + \xi_5(z_h - z_{cg}))\rho C_T V_0$, where $\rho C_T V_0$ represents an aerodynamic damping coefficient for a FOWT, B_{aero}. Note that, the second order and the higher terms in Eq. (3) are discarded.

To obtain the motions of a FOWT to combined waves and wind loads in frequency domain, the aerodynamic forces on the rotor should be added to the equation of motion, Eq. (1). Of the two terms of the total thrust force on a FOWT, Eq. (3), the forces due to the aerodynamic damping are harmonic. Hence, we need to approximate the aerodynamic excitation force on the fixed rotor by a harmonic function with the same frequency as the incident waves. Since the integrated aerodynamic normal force over the rotor acts at the hub centre and it is transferred to the tower top, and the cross-section at the top of the tower is circular, we can obtain the phase angle of the excitation aerodynamic force following the same approach as presented by MacCamy and Fuchs (1954), [9], for wave-interaction with a circular cylinder *i.e.*

$$F_{1,W} = \frac{1}{2}C_T\rho V_0^2 A_r \cos(\omega t - \delta_{\text{aero}}), \tag{4}$$

where $F_{1,W}$ is the aerodynamic excitation force on a rotor in surge and δ_{aero} is the phase angle of the inline force:

$$\delta_{\text{aero}}(kr_0) \ = \ -\tan^{-1}\big[\frac{Y_1^{'}(kr_0)}{J_1^{'}(kr_0)}\big], \tag{5}$$

where k is the wave number, r_0 is the top diameter of the tower and $J_1(kr)$ and $Y_1(kr)$ are the Bessel functions of the first and the second kind of order 1, respectively.

The excitation aerodynamic load vector, F_W, and the aerodynamic damping matrix, $B_{aero,mat}$ on the rotor are added to the right-hand side and the left-hand side of the equation of motion of a floating platform in frequency domain, Eq. (1), respectively. The motions of a FOWT to combined waves and wind loads are determined as,

$$\xi_j[-\omega^2(M_{ij}+a_{ij})+i\omega(\,b_{ij}+B_{aero,mat}\,)+(\,c_{ij,moor}+c_{ij})] \ = \ AX_i + F_W\,, \quad i,j = 1,2,\cdots m. \tag{6}$$

For hydro- and aero-analysis of a FOWT, a finite element model of the complete structure is prepared and the mode-shapes of the FOWT are determined. The mode-shapes of the fully flexible FOWT are added as generalized modes to the rigid-body degrees of freedom of the structure. Moreover, the hydrostatic restoring coefficients of a flexible FOWT are computed with a complete formulation developed in [10] and includes the effects of both changes in the hydrostatic pressure and the structural geometric stiffness.

The numerical solution of the formulations discussed above are obtained in HYDRAN-XR (see [11]), a potential flow solver that is integrated with finite element analysis. HYDRAN-XR is modified to include the aerodynamic analysis of one or multiple wind turbines on a floating platform. The total aerodynamic excitation load vector consists of aerodynamic loads on the rotor and the tower. The aerodynamic loads on the tower are computed with an empirical relation for the drag force with respect to the incoming wind Reynolds number. The aerodynamic excitation and damping forces are distributed as nodal forces on the front face of the rotor rather than integrated forces at the hub centre. Similarly, the aerodynamic load on the tower is distributed on the front face of the tower. In the end, the elastic motions of a FOWT to combined waves (regular and irregular) and wind loads are obtained in HYDRAN-XR.

3. Results & discussion

The hydro-aero-elastic motions of two FOWTs, namely a SPAR FOWT and a multi-unit FOWT to irregular waves, and combined irregular waves and wind, are presented. The irregular waves are developed by adopting JONSWAP spectrum with three modal wave periods, shown in Fig. 1. In this section, first, the significant motions of the rigid SPAR FOWT to irregular waves and combined irregular waves and steady wind are computed with the results of HYDRAN-XR and compared with laboratory measurements and available numerical results. Next, the multi-unit FOWT is described and its rigid- and flexible body motions to waves (regular and irregular), and combined waves (regular and irregular) and wind loads are provided. The SPAR and the wind-tracing FOWTs are with 8082 and 9792 constant source fluid panels, respectively. The simulations are conducted on a desktop machine with Intel Core *i5*, 3.20 GHz CPU and 32 GB memory and took approximately 4.5 hours for the SPAR FOWT and 11 hours for the wind-tracing FOWT, respectively.

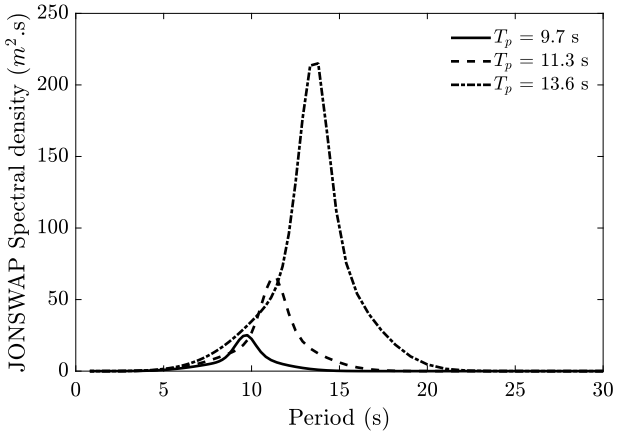

Figure 1 The JONSWAP frequency spectrum with three modal periods, $T_p = 9.7$ s, $T_p = 11.3$ s and $T_p = 13.6$s with cut-off frequency of 1.25 rad/s.

3.1. The SPAR FOWT

In OC3 project [12] a SPAR FOWT supporting a 5 MW NREL wind turbine [13] is introduced and studied. Ahn and Shin [14] conducted laboratory measurements on motions of a model of the SPAR FOWT with a scaling ratio of $1:128$ to regular and irregular waves with parked and operating wind turbine. In these experiments, the incoming wind speed is 1.007 m/s with operating model rotor at 136.9 rpm corresponding to the rated wind speed of the 5 MW NREL prototype, 11.4 m/s and operating prototype rotor at 12.1 rpm. The irregular waves are modelled with the JONSWAP spectrum with three modal wave periods, $T_p = 9.7$ s, 11.3 s and 13.6 s. Ahn and Shin measured the significant motions of the model SPAR FOWT to irregular waves and combined irregular waves and rated wind speed, and computed the responses of the structure to the same environmental loading by an in-house numerical model at University of Ulsan, namely the UoU+FAST v8 numerical tool.

The rigid SPAR FOWT is modelled with respect to its prototype dimensions in HYDRAN-XR. The mass matrix, viscous damping coefficients, and the properties and configuration of the mooring lines are defined as given in [12]. Shown in Fig. 2, the significant motions of the structure to irregular waves and combined irregular waves and wind at 11.4 m/s are computed and compared with laboratory measurements and numerical results of [14]. The numerical results by HYDRAN-XR are in a very good agreement with the laboratory measurements for combined irregular waves and wind loads. However, considering the irregular wave loads with wave period of $T_p = 13.6$ s, the numerical results of both HYDRAN-XR and UoU+FAST v8 are overestimated compared with the laboratory measurements.

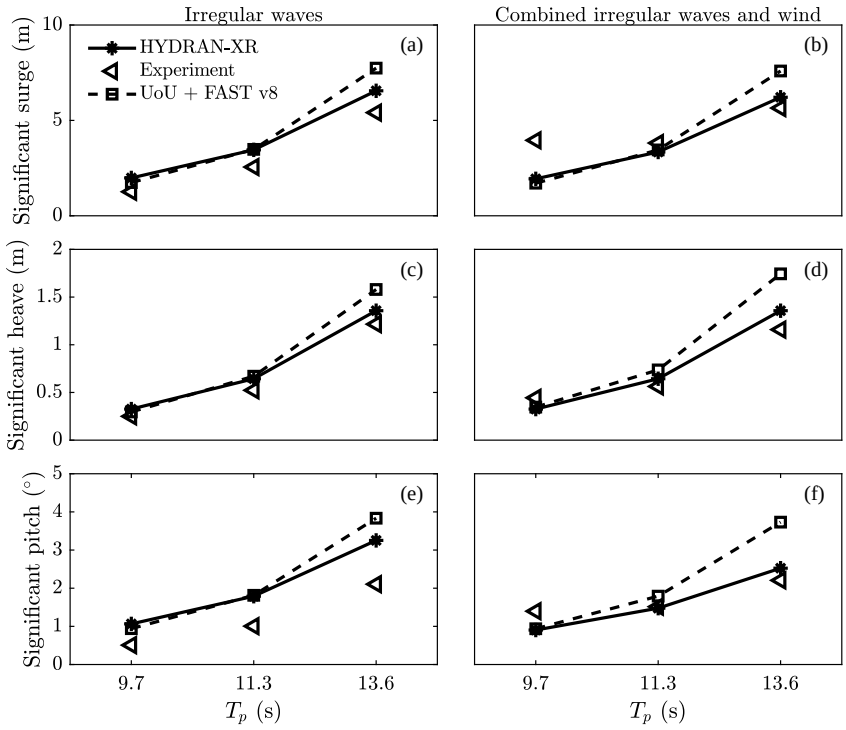

Figure 2 Comparison of the significant motions of the OC3 SPAR FOWT to irregular waves, and combined irregular waves and wind loads computed by HYDRAN-XR, and laboratory measurements and numerical results by UoU+FAST v8 of Ahn & Shin [14]. The irregular waves are developed with JONSWAP spectrum and modal periods of $T_p = 9.7$ s, $T_p = 11.3$ s and $T_p = 13.6$ s.

3.2. The wind-tracing FOWT

In this section, the responses of a multi-unit, wind-tracing FOWT to combined waves and wind loads are presented. In this study, first, a short discussion is provided on the motions of the wind-tracing FOWT to regular waves and combined regular waves and wind loads. Next, the significant motions of the rigid and the flexible structures to irregular waves (with JONSWAP spectrum) and combined irregular waves and wind loads are presented and discussed. The aerodynamic loads on the rotors and the towers are computed for incoming wind speed at 11.4 m/s and rotor operating at 12.1 rpm.

The wind-tracing FOWT introduced in [15] consists of an equilateral triangular platform that supports three 5 MW NREL wind turbines at its corners. The water ballast is distributed within closed compartments in the columns and at the middle of the pontoons. Dimensions and the wall thicknesses of the columns and the pontoons are described in [5] and [16]. The pontoons are $2.2\ D_r$ long, where D_r is the diameter of the rotors. The length of the pontoons is specified such that the interaction of the rear and the front wind turbines on the wind-tracing platform is minimized. The wind-tracing FOWT is connected to a turret-bearing system, submerged under the platform. The turret-bearing mooring system allows the structure to rotate to the direction of the dominant incoming wind load with respect to the turret. Finally, the turret is moored to the seabed with four catenary mooring lines, see [16] for more details. The mode-shapes of the wind-tracing FOWT and its hydroelastic responses to regular waves, and aligned and misaligned regular waves and wind loads, are investigated and discussed in detail in [17]. In a parametric study, [17] the motions of the wind-tracing FOWT with several configurations of the turret-bearing mooring system are investigated. For the preferred configuration of the mooring system, the turret is submerged for $4\ d$ under the platform, where $d = 16$ m is the draft of the wind-tracing FOWT and a distance of $1/6L$ from the rear column, where L is the horizontal distance between the rear column and the front pontoon.

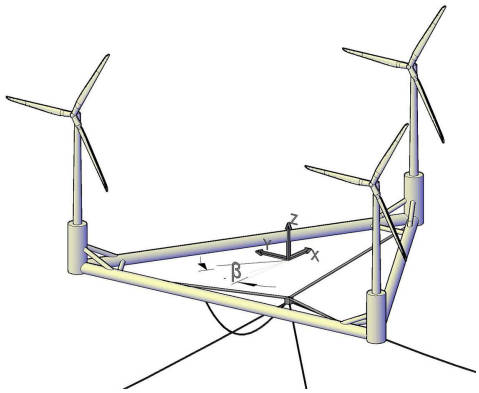

Figure 3 Schematic of the wind-tracing FOWT. β indicates the wave heading angle.

The finite element model of the wind-tracing FOWT is prepared and its hydro- and aeroelastic motions, and significant responses to waves, and combined waves and wind loads are obtained. The governing equation of motion, Eq. (6) is solved for 10 modes, *i.e.* six rigid body modes and four generalised modes representing the first four dry modes of the FOWT. The considered generalised modes are mainly dominated by edgewise and flapwise deflections of the blades and the side-side deflections of the towers where the deflection along the pontoons are very small; see [17] for more details. The dry natural periods of the model included were between 3.9 s and 6.5 s. The wet natural periods of the wind-tracing FOWT at its first four generalised modes occur in short wave periods and are 7.208 s, 7.244 s, 7.92 s and 7.988 s. In this study, the wind load is orthogonal to the rotor and the tower, and the wave heading angle changes to represent misaligned wave and wind loads. Figures 4 and 5 show the comparison of the response amplitude operators (RAOs) of the wind-tracing FOWT to regular waves, and regular waves and wind loads for wave heading angles $\beta = 0^\circ$ and $\beta = 90^\circ$.

Shown in Fig. 4, the surge RAOs of both rigid and flexible structures are comparable for both wave heading angles. The surge motions of the structure is larger to the incident waves with zero wave heading angle compared to those with $\beta = 90^\circ$. Furthermore, the flexible structure undergoes some small peaks for 7 s $\leq T \leq 10$ s, where the four generalised wet natural periods of the wind-tracing FOWT are. The heave RAOs of the rigid and flexible wind-tracing FOWT are in agreement for wave periods smaller than approximately 17 s. The heave responses of the rigid structure for both wave heading angles undergo three peaks at approximately 20.44 s, 21.42 s, 27.78 s where they are the pitch, roll and heave natural periods of the rigid wind-tracing FOWT. However, the coupling between the heave and roll and pitch in heave motions of the flexible wind-tracing FOWT is not observed and the flexible body heave RAOs experience only a peak at 26.74 s, the heave natural period of the flexible wind-tracing FOWT. The pitch RAOs of the structure for $\beta = 90^\circ$ are slightly smaller than the pitch motions for headseas. Similar to the heave motions of the rigid structure, the rigid-body pitch RAOs show two peaks at 20.44 s and 21.42 s. In contrast, the flexible wind-tracing FOWT undergoes a peak at 21.10 s, the pitch and roll natural periods of the flexible wind-tracing FOWT.

The surge motions of the flexible wind-tracing FOWT due to combined waves and wind loads are larger compared with its rigid-body counterparts, see Fig. 5. Furthermore, the peaks of the flexible wind-tracing FOWT in surge at the vicinity of its generalised wet natural periods are slightly larger compared with the rigid body. Moreover, the addition of the aerodynamic forces on the rigid and flexible FOWTs results in larger peaks in pitch for both wave heading angles.

The significant motions of the wind-tracing FOWT to irregular waves (JONSWAP spectrum) and combined irregular waves and steady wind loads are computed for aligned and misaligned waves and wind loads with $0^\circ < \beta < 180^\circ$. The significant motions are presented as a function of the wave heading angles and for three modal wave periods $T_p = 9.7$ s, $T_p = 11.3$ s and $T_p = 13.6$ s, in Figs. 6 and 7 for waves and wave-wind combined conditions, respectively. Commonly, the significant motions of the

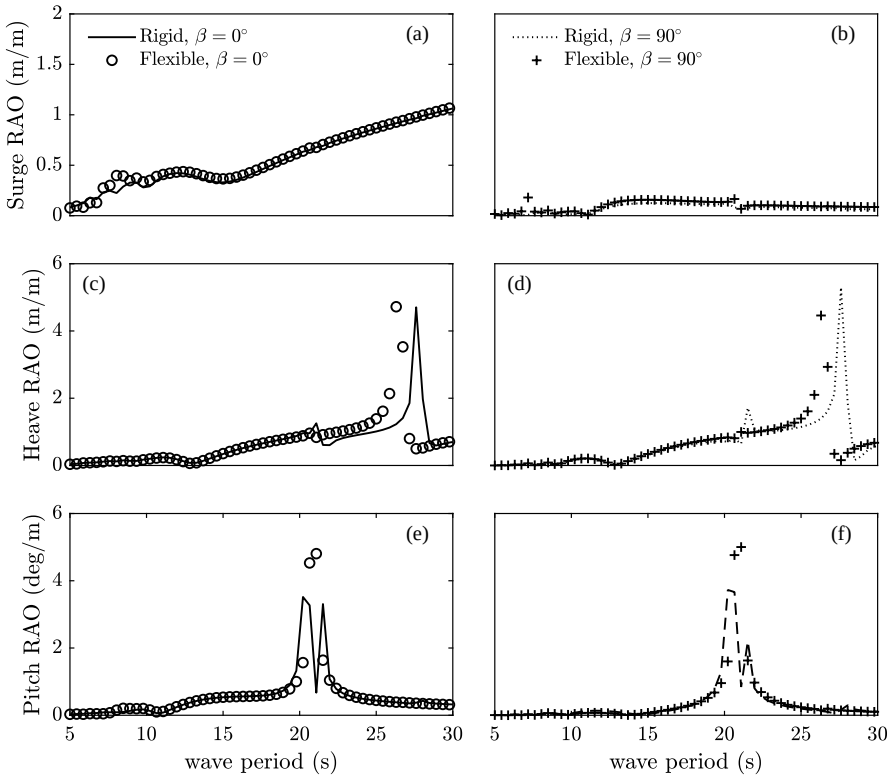

Figure 4 Comparison of the wave-induced RAOs of the rigid and fully flexible wind-tracing FOWT for two wave heading angles $\beta = 0°$ and $90°$.

structure in surge, heave and pitch increase as the modal wave period increases. The motions of the flexible FOWT in surge are slightly larger than the rigid wind-tracing FOWT at the three modal wave periods. Similarly as shown in Fig. 4, at the modal wave periods, i.e. $T_p = 9.7$ s, $T_p = 11.3$ s and $T_p = 13.6$, the surge RAOs of the flexible structure to wave loads are larger than the rigid wind-tracing FOWT. Regarding the heave significant motions, the difference between the flexible and rigid structures is the largest at $T_p = 13.6$ s, where the flexible structure shows larger significant motions. Moreover, the pitch significant motions of the rigid and the flexible wind-tracing FOWTs agree well for $\beta < 60°$ and $\beta > 110°$, while for $60° < \beta < 110°$ the flexible structure undergoes smaller significant pitch motions compared with the rigid structure.

Shown in Fig. 7, due to the addition of the aerodynamic loads, the significant motions of the rigid structure in surge are slightly smaller than its counterparts by the flexible wind-tracing FOWT. Since the aerodynamic forces on the structure are parallel with *x*-axis, and act in *xz*-plane, the significant heave motions of the structure experience very small changes for the three modal wave periods compared with the heave motions due to wave loads, presented in Fig. 6. Moreover, the pitch significant motions of the rigid wind-tracing FOWT are smaller in comparison with the flexible structure for modal wave periods $T_p = 9.7$ s and $T_p = 11.3$ s.

4. Concluding remarks

In this study, the significant motions of a single- and a multi-unit FOWT to irregular waves and combined irregular waves and wind loads are presented. A numerical coupling approach is described to obtain the hydro- and aeroelastic motions of FOWTs to waves and wind loads. The numerical approach is implemented in a potential flow solver integrated with finite element analysis, HYDRAN-XR. HYDRAN-XR is enhanced to include aerodynamic analysis of FOWTs.

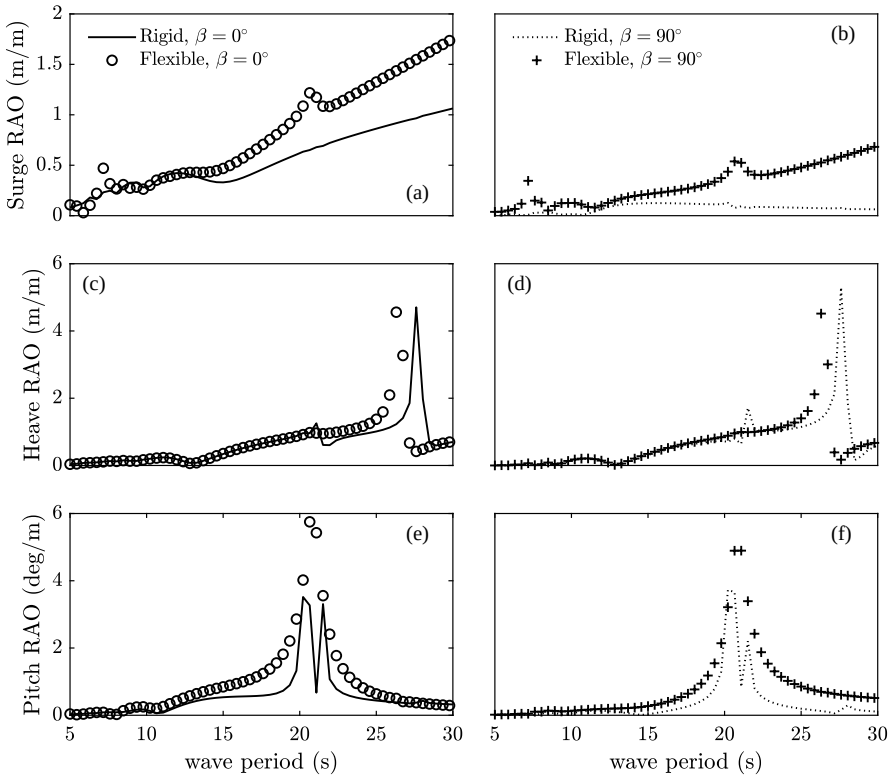

Figure 5 Comparison of the RAOs of the rigid and fully flexible wind-tracing FOWT to combined waves and wind loads for two wave heading angles $\beta = 0°$ and $90°$.

First, the rigid body significant motions of a SPAR FOWT to irregular waves, and irregular waves and wind loads are presented and compared with laboratory measurements and existing numerical solutions. Very good agreement between the numerical results by HYDRAN-XR and the laboratory measurements is observed. Next, the rigid- and flexible-body motions of a multi-unit FOWT, the wind-tracing FOWT to regular wave and combined regular waves and wind loads are presented and discussed. It is shown that the flexible structure experiences slightly smaller and larger natural periods in heave and pitch modes, respectively. Next, the significant motions of the rigid and flexible wind-tracing FOWT to irregular waves (JONSWAP spectrum) and aligned and misaligned irregular waves and wind loads are presented. It is shown that the significant motions of the flexible wind-tracing to irregular waves, and combined irregular waves and wind in surge and heave are larger than its counterparts by the rigid structure.

Determining the complex motions of multi-unit FOWTs to the environmental loads is challenging. This study indicates that the responses of a rigid multi-unit FOWT to irregular waves and combined irregular waves and wind loads might be substantially different while considering the flexibility effects of the entire structure.

Acknowledgments

The work of AL and MH is partially based on funding from the CBJ Ocean Engineering Corp. of Hong Kong. This funding is gratefully acknowledged. Any findings and opinions contained in this paper are those of the authors and do not necessarily reflect the opinions of the funding company.

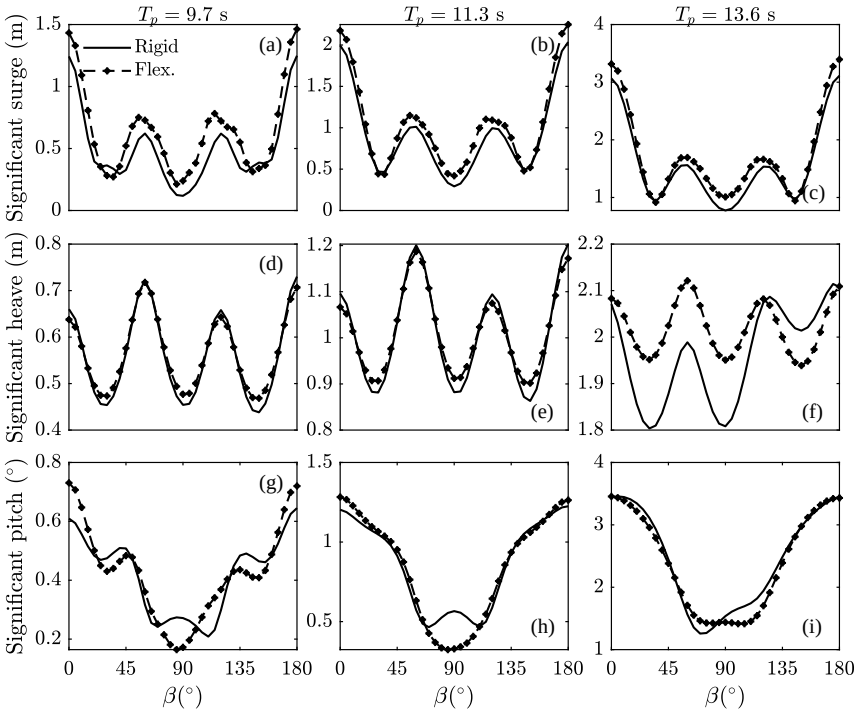

Figure 6 The significant motions of the rigid and flexible wind-tracing FOWT to irregular waves with wave heading angles $0° < \beta < 180°$. The irregular waves are developed with JONSWAP spectrum and modal periods of $T_p = 9.7$ s (left column), $T_p = 11.3$ s (middle column) and $T_p = 13.6$ s (right column).

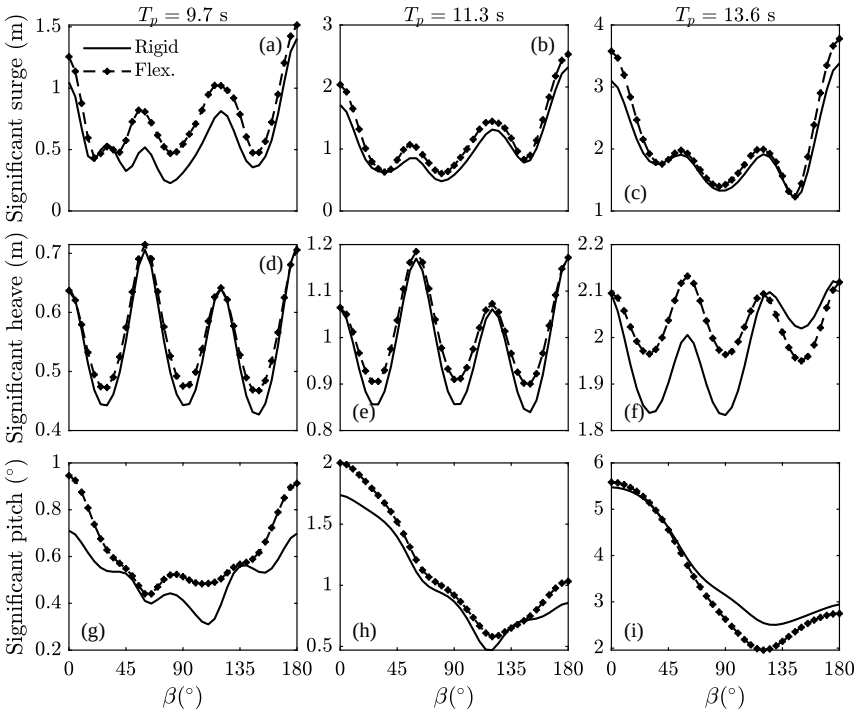

Figure 7 The significant motions of the rigid and flexible wind-tracing FOWT to combined irregular waves and wind loads with wave heading angles $0° < \beta < 180°$. The irregular waves are developed with JONSWAP spectrum and modal periods of $T_p = 9.7$ s (left column), $T_p = 11.3$ s (middle column) and $T_p = 13.6$ s (right column).

References

[1] V. Arramounet, C. E. de Winter, N. Maljaars, S. Girardin, and H. Robic. Development of coupling module between BHawC aeroelastic software and OrcaFlex for coupled dynamic analysis of floating wind turbines. *Journal of Physics: Conference Series*, 1356(1):1–10, doi:10.1088/1742–6596/1356/1/012007, 2019.

[2] K. Jessen, K. Laugesen, M. Signe Mortensen, K. J. Jensen, and N. M. Soltani. Experimental validation of aero-hydro-servo-elastic models of a scaled floating offshore wind turbine. *Applied Sciences*, 9(6):1–28, doi:10.3390/app9061244, 2019.

[3] H. K. Jang, H. C. Kim, M. H. Kim, and K. H. Kim. Coupled dynamic analysis for multi-unit floating offshore wind turbine in maximum operational and survival conditions. In *Proceedings of the 34th International Conference on Offshore Mechanics and Arctic Engineering - OMAE*, pages 1–8, doi:10.1115/OMAE2015–42062, May 31-June 5, Newfoundland, Canada, 2015. ASME.

[4] H. Y. Kang, M. H. Kim, K. H. Kim, and K. Y. Hong. Hydroelastic analysis of multi-unit floating offshore wind turbine platform (MUFOWT). In *Proceedings of the 27th International Offshore and Polar Engineering Conference*, pages 554–560, June 25-30, San Francisco, CA, USA, 2017. ISOPE.

[5] A. Lamei, M. Hayatdavoodi, C. Wong, and B. Tang. On motion and hydroelastic analysis of a floating offshore wind turbine. In *Proceedings of the 38th International Conference on Offshore Mechanics and Arctic Engineering - OMAE*, pages 1–10, doi:10.1115/OMAE2019–96034, June 9-14, Glasgow, UK, 2019. ASME.

[6] M. Borg, H. Bredmose, and A. M. Hansen. Elastic deformations of floaters for offshore wind turbines: Dynamic modelling and sectional load calculations. In *Proceedings of the 36th International Conference on Offshore Mechanics and Arctic Engineering - OMAE*, pages 1–10, doi:10.1115/OMAE2017–61446, June 25-30, Trondheim, Norway, 2017. ASME.

[7] A. Lamei and M. Hayatdavoodi. On motion analysis and elastic response of floating offshore wind turbines. *Journal of Ocean Engineering and Marine Energy*, 6(1):71–90, doi:10.1007/s40722–019–00159–2, 2020.

[8] A. Lamei, M. Hayatdavoodi, and H. R. Riggs. On coupling wave- and wind-induced hydroelastic and aeroelastic responses of floating offshore wind turbines (revision submitted). *Marine Structures*, 2022.

[9] R.C. MacCamy and R.A. Fuchs. *Wave forces on piles: A diffraction theory*. Tech. Memo. No. 69. Beach Erosion Board. Army Corps of Engineers, 1-17, 1954.

[10] L. L. Huang and H. R. Riggs. The hydrostatic stiffness of flexible floating structures for linear hydroelasticity. *Marine Structures*, 13:91–106, doi:10.1016/S0951–8339(00)00007–1, 2000.

[11] NumSoft Technologies. HYDRAN-XR, hydrodynamic response analysis with integrated structural finite element analysis, version 20.1. Technical report, Numsoft Technologies, 2020.

[12] J. M. Jonkman. Definition of the floating system for phase IV of OC3, accessed: December 2020. Technical report, National Renewable Energy Laboratory (NREL), Golden, CO, USA, doi:10.2172/979456, 2010.

[13] J. M. Jonkman, S. Butterfield, W. Musial, and G. Scott. Definition of a 5-MW reference wind turbine for offshore system development, accessed: December 2020. Technical report, National Renewable Energy Laboratory (NREL), Golden, CO, USA, doi:10.2172/947422, 2009.

[14] H. J. Ahn and H. Shin. Model test and numerical simulation of OC3 SPAR type floating offshore wind turbine. *International Journal of Naval Architecture and Ocean Engineering*, 11(1):1–10, doi:10.1016/j.ijnaoe.2017.09.010, 2017.

[15] C. Wong. Wind-tracing rotational semi-submerged raft for multi-turbine wind power generation. In *European Wind Energy Association Offshore 2015 Conference*, pages 1–10, March 10-12, Copenhagen, Denmark, 2015.

[16] S. Li, A. Lamei, M. Hayatdavoodi, and C. Wong. Concept design and analysis of wind-tracing floating offshore wind turbines. In *Proceedings of the ASME 2019 2nd International Offshore Wind Technical Conference, November 3-6, St. Julian's, Malta*, pages 1–8. ASME, 2019.

[17] A. Lamei, M. Hayatdavoodi, and H. R. Riggs. Motion and elastic response of wind-tracing foating offshore wind turbines (under review). *Journal of Ocean Engineering and Marine Energy*, 2022.